Arcjet Engine Performance: Experiment and Theory

RICHARD R. JOHN,* STEWART BENNETT,† AND JOHN F. CONNORS‡
Avco Corporation, Wilmington, Mass.

Analytical and experimental results are presented on the propulsion performance and the energy addition and loss mechanisms of a radiation-cooled arcjet engine having a constricted-arc configuration. A useful lifetime of one month has been obtained with such an engine operated with hydrogen at 1000-sec specific impulse, 30-kw d.c. power input, and an electric to thrust power conversion efficiency of 40%. At 30-kw input power, reliable engine operation was obtained at up to 1000-sec specific impulse with ammonia and up to 1500-sec specific impulse with hydrogen. Specific impulses greater than 2000 sec were obtained using hydrogen in a radiation-cooled engine operated at 200-kw input power. Electric to thrust power conversion efficiencies were in the range from 35 to 45%. Visual examination of the arc discharge through a quartz constrictor indicated that there was a smooth, constant-diameter, luminous core extending from the cathode through the constrictor and terminating in the nozzle. Examination of experimental cool-off data and engine exterior surface temperature distributions indicated the existence of an energy transfer path from the hot engine walls to the cold incoming propellant.

OF the wide variety of electric propulsion schemes currently under analytical and experimental investigation, the thermal arcjet is probably nearest to hardware realization. The object of this paper is to present the results of recent experiments and analysis pertinent to the conversion of the laboratory thermal arcjet into an efficient and reliable device suitable for missions in space.

I. Engine Configuration and Operation

A cutaway view of a direct current radiation-cooled arcjet engine typical of the type used in the experimental program is shown in Fig. 1. The cathode and anode are thoriated tungsten. The insulator is boron nitride, and the gas injection plenum is molybdenum. Gas seals are provided by metal *c*-rings.

A schematic view of the engine internal configuration is presented in Fig. 2. The gaseous propellant is injected through a series of critical flow orifices into the annular space surrounding the central tungsten cathode. The arc discharge extends from the cathode tip through a constant area constrictor section and terminates in the expansion portion of the exit nozzle. The usual plenum chamber has been eliminated in order to minimize convective heat transfer losses.

Both capacitor and high-frequency discharges have been used for arc initiation; these methods are effective but require auxiliary starting systems. A simpler method for arc initiation is based on Paschen's law.[1] Briefly, Paschen's law is a statement of the empirical fact that the spark breakdown voltage for a given gas is a function of the product of electrode separation (gap length) and pressure; this breakdown voltage is a minimum at a particular value of the product of gap length and pressure. In a test tank or space environment, before there is any propellant flow the product of gap length and gas pressure is essentially zero. As the propellant begins to flow, the pressure across the arc gap increases; therefore, the product of gap length and gas pressure increases, and there is a corresponding decrease in the breakdown voltage. When the required gap breakdown voltage falls below the applied open circuit voltage, the arc is initiated spontaneously.

This starting technique has been successfully applied to electric arc plasma generators in the power range from 1 to 500 kw and was used for starting engines in the experiments described below. The minimum required applied open circuit voltage for arc initiation was 275 v.

II. Engine Steady-State Propulsion Performance

A. Thrust Measurement System

A critical problem in any electric propulsion program is the accurate laboratory measurement of low values of thrust from a high-temperature electric propulsion device for extended time periods (order of days and even months). The thrust stand must be insensitive to the thermal loads produced by the electric propulsion engine. The thrust stand shown schematically in Fig. 3 is an effort to solve this problem.

Referring to Fig. 3, the plasmajet engine (12) is permanently mounted on the oil container (13), which in turn is mounted on the stationary plate (6) by means of four thin steel strips (10). Any thrust produced by the plasmajet engine results in displacement of the engine and oil container until a point is reached such that the restoring force produced by the thin steel strips balances the engine thrust. The absolute displacement of the plasmajet engine is recorded by the dis-

Some of the material presented here is contained in papers by the authors presented at the ARS 17th Annual Meeting and Space Flight Exposition, Los Angeles, Calif., November 13–18, 1962, the AIAA Electric Propulsion Conference, Colorado Springs, Colo., March 11–13, 1963, and the AIAA Summer Meeting, Los Angeles, Calif., June 17–20, 1963; revision received August 21, 1963. The work described in this paper was supported by the NASA Lewis Research Center, Cleveland, Ohio, under NASA Contract No. NAS 5-600.

* Assistant Manager, Research and Advanced Development Division, Aerophysics Department. Member AIAA.

† Senior Staff Scientist, Research and Advanced Development Division, Aerophysics Department. Member AIAA.

‡ Group Leader, Research and Advanced Development Division, Aerophysics Department.

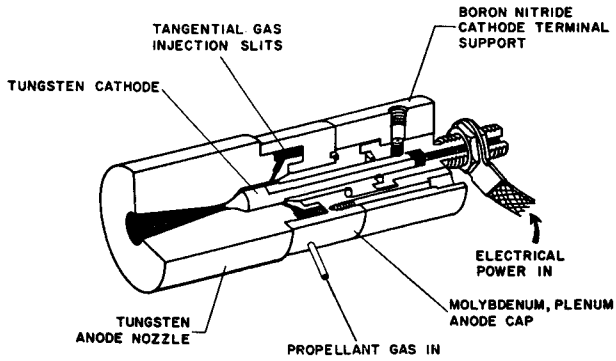

Fig. 1 Schematic diagram of 30-kw radiation-cooled arcjet engine.

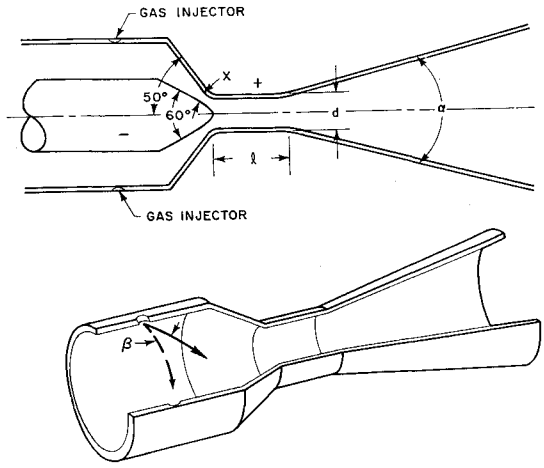

Fig. 2 Basic constricted-arc configuration.

placement transducer (8). To avoid errors due to extraneous thermal loads from the hot plasmajet engine or other sources, the steel strips and the displacement transducer are completely immersed in a constant-temperature silicone oil bath (5). The silicone oil is held in the oil container, and the oil temperature is held constant by means of the heat exchanger (11).

The thrust stand was calibrated before and after a run by a string, pulley, and weight system. Provision was also made for checking the incremental calibration of the thrust stand during the course of a run by adding or subtracting standard weights. The null-setting of the thrust stand remained constant when the engine was short-circuited (to check possible magnetic field effects) at rated current.

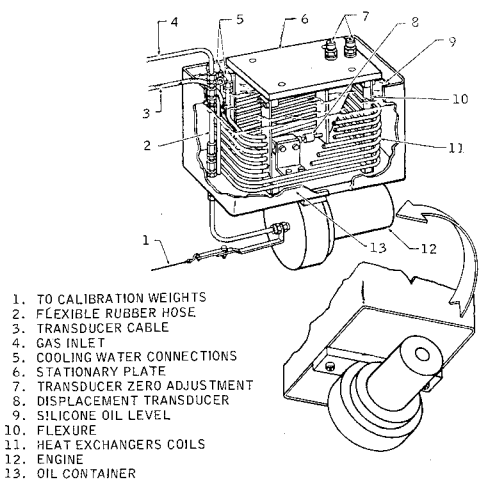

Fig. 3 Water-cooled thrust stand for testing radiation-cooled arcjet engines.

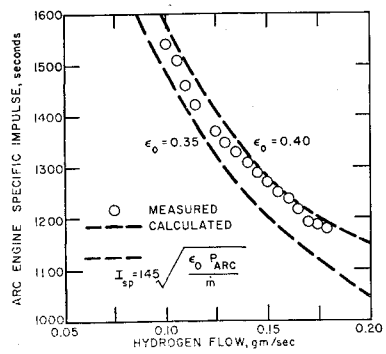

Fig. 4 Specific impulse vs hydrogen flow rate for a radiation-cooled arcjet engine operated at 30-kw input power.

The response of the stand (i.e., output of the displacement transducer) was observed to be linear with applied thrust; the accuracy of the unit was estimated to be ±3%, and the time response was about 1 sec. Thermocouple measurements on the support structure between the engine and oil bath container indicated that the heat leak between the engine and the silicone oil was less than 100 w for the radiation-cooled 30-kw arcjet engine. This is not considered sufficient to affect engine performance.

The thrust stand was mounted in a double-walled test chamber with water-cooled walls and viewing ports. The chamber (2 ft in diam and 8 ft long) was connected to a 6500-ft³/min pumping system. The exhaust gases from the arc engine passed over a heat exchanger located within the test tank; the exhaust propellant therefore entered the vacuum pumps at about room temperature. The pumps were filled with a nonhydrogenating oil.

The rate of propellant flow to the engine was measured by means of a rotameter, which in turn was calibrated by a standard gas displacement technique. Direct current power was supplied to the engine from a 320-v (open-circuit voltage) selenium rectifier power supply equipped with a magnetic amplifier for power control and was measured with precision voltmeters, ammeters, and wattmeters. The flow and power measurement are each estimated to be accurate to about ±3%.

B. Performance Data

Steady-state performance data for a hydrogen-fueled radiation-cooled arcjet engine, having a nominal power rating of 30 kw, are shown in Fig. 4. Measured engine steady-state specific impulse is plotted as a function of hydrogen flow rate. Superimposed on the experimental results are curves

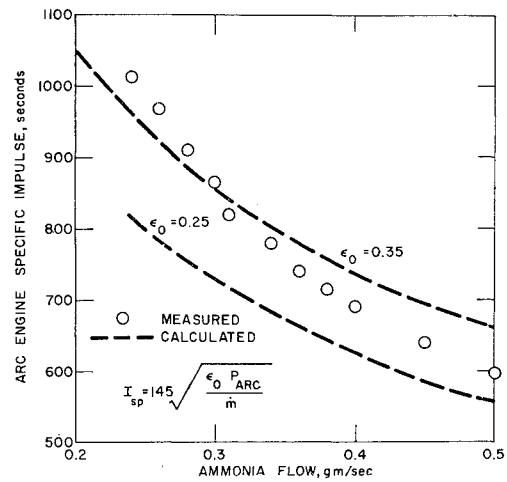

Fig. 5 Specific impulse vs ammonia flow rate for a radiation-cooled arcjet engine operated at 30-kw input power.

Table 1 Maximum specific impulse obtained with radiation-cooled arcjet engines having a constricted arc configuration

Nominal power, rating, kw	30	30	215
Working fluid	H_2	NH_3	H_2
Arc current, amps	150	280	1350
Arc voltage, v	200	107	160
Propellant flow rate, g/sec	0.10	0.25	0.33
Over-all efficiency, %	38	40	35
Maximum specific impulse, sec	1550	1000	2200

for different assumed over-all energy conversion efficiencies determined from the energy balance relation

$$I_{sp} = 4.56(\epsilon_0 IV/\dot{M})^{1/2} \quad (1)$$

where $\dot{M}$ is the mass flow (grams per second), I is the engine current (amperes), V is the arc voltage (volts), and ϵ_0 is the over-all energy conversion efficiency. The experimental data fall close to the calculated specific impulse curve corresponding to an assumed electric-to-thrust power efficiency of 40%. The experimental electric-to-thrust power conversion efficiency increases slightly with increase in specific impulse. This observed efficiency behavior is in marked contrast to the strong efficiency fall-off predicted on the basis of one-dimensional frozen flow considerations.[2]

A similar insensitivity of over-all energy conversion efficiency to specific impulse is shown on the performance curve for the 30-kw ammonia-fueled radiation-cooled arcjet engine presented in Fig. 5. Because of its higher molecular weight and thus higher inherent operating temperatures, the maximum operating specific impulse for ammonia is considerably lower than that for hydrogen.

Table 1 presents values of the maximum specific impulse obtained with a series of radiation-cooled arcjet engines of different design power levels but of the general type shown in Figs. 1 and 2. All the data have been obtained under steady-state operating conditions.

The results shown in Table 1 represent empirical state-of-the-art data and are not to be considered as a fundamental upper limit to arc engine performance.

C. Life and Reliability

A summary of experimental data obtained during a series of long-duration radiation-cooled arc engine runs is shown in Table 2.

No dimensional changes were observed in the constrictors of any of the engines used in the long-duration runs. This observation strongly suggests that the arc discharge originated at the cathode and terminated in the exit nozzle expansion section. The anode-nozzle weight loss was in all cases 0.1% or less of the total anode-nozzle weight. Cathode weight losses reached a maximum of 1% of the total cathode weight. The major portion of the cathode weight loss probably occurred during the first 10 or 20 hr of engine operation, although this point is still being investigated.

The indicated values of maximum exterior surface temperature are based on optical pyrometer measurements of the engine brightness temperature. From heat-conduction considerations, with the assumption that the interior heat-transfer distribution is not sharply localized, the temperatures characteristic of the engine interior are probably a maximum of 200° or 300°K greater than the measured surface temperature. These estimated peak interior temperatures are considerably below the melting point of tungsten (3650°K). Thus, engine operation at specific impulses greater than the values shown in Tables 1 and 2 is probably not limited by the melting point of tungsten but by the high-temperature strength capability of the engine metal to metal braze joints. The specific impulse capability of the radiation-cooled arcjet engine can, therefore, probably be increased above the maximum value of 1500 sec shown in Table 2 by either changing the location or increasing the high-temperature strength capability of the braze joints.

III. Mechanisms of Energy Addition and Loss

The conventional one-dimensional analysis of the nozzle expansion process in the arcjet rocket engine is based on the assumption that the flow enters the nozzle from a plenum chamber; the thermodynamic state of the gas entering the exit nozzle is established by the stagnation enthalpy and pressure of the gas in the plenum and is a function only of axial nozzle distance. In the constricted arc design, shown in Fig. 1, the plenum has been eliminated with the result that the flow passing through the engine is spatially nonuniform; the thermodynamic state of the expanding gas is a function of both distance along the nozzle axis and radial distance from the nozzle axis.

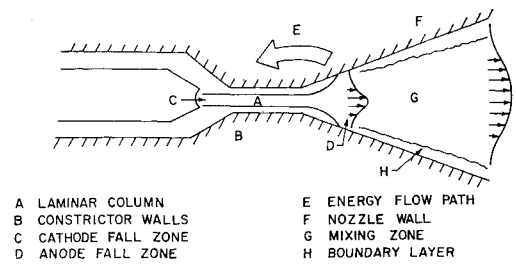

Fig. 6 Core flow model of the energy transfer processes in a radiation-cooled arcjet engine.

A. Core Flow Model

Referring to Fig. 6, basic assumptions underlying a proposed core flow model for description of the arc engine nonuniform energy transfer process are as follows:

1) The arc discharge fills only a small fraction of the constrictor cross section. The central arc discharge runs the length of the constrictor (B) from the cathode fall zone (C) to the anode fall zone (D).

2) The positive terminus of the arc discharge, which is located in the expansion portion of the nozzle, is diffuse and thus conducive to prolonged anode life.

3) The portion of the propellant which is not heated by direct contact with the arc column is heated by contact with

Table 2 Summary of long-duration runs of radiation-cooled arcjet engines operated at 30 kw input power with hydrogen

Specific impulse, sec	Over-all efficiency, %	Run duration, hr	Maximum measured exterior temperature, °K	Cathode loss,[a] g	Anode loss, g	Run termination
1000	41	723 (one month)	1800	0.67	0.22	voluntary
1320	44	250	2200	0.60	<0.01	voluntary

[a] The cathode had a nominal weight of 100 g, and the anode had a nominal weight of 1500 g.

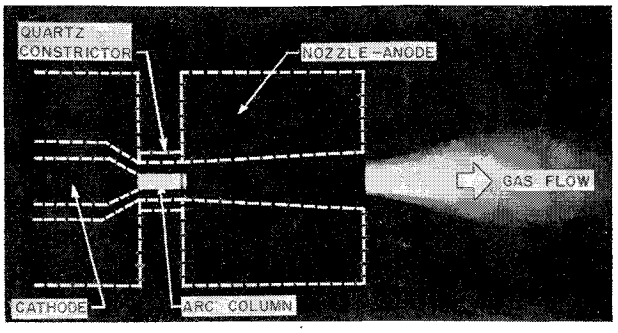

Fig. 7 Photograph of the arc discharge obtained through a quartz constrictor. Arc voltage, 150 v; arc current, 150 amps; hydrogen flow, 0.25 g/sec.

the engine walls. Heat is transferred along a thermal conduction path (E) through the engine from the hot regions around the nozzle (F) to the cooler regions near the constrictor.

4) The flow entering the nozzle is highly nonuniform and consists of a central hot portion that has been heated by direct contact with the column and an outer portion heated by contact with the engine walls.

Analytical and experimental evidence substantiating the existence of a central core flow is presented below.

B. Characteristics of the Visible Arc Discharge

An experimental arcjet engine has been fabricated with the modification that the constrictor is made of a quartz tube that permits visual access to the discharge. A photograph of the discharge obtained through the constrictor is shown in Fig. 7. A smooth central column extends from the vicinity of the cathode to the end of the constrictor. This luminous core has a remarkably constant diameter that is less than the constrictor diameter. The quartz constrictor has been observed to stand up for periods of minutes, suggesting that the gas flow next to the constrictor wall is relatively cool.

Preliminary spectroscopic measurements have been carried out to determine temperature profiles across the visible column. As an initial effort, a photographic technique, based on a method developed by Larentz[3] and Olsen,[4] has been used. Briefly, a photograph of the arc column was obtained through a filter centered about the alpha line of the Balmer series (6563Å). The emission intensity distribution $S(X)$ was determined from a densitometer trace of the photograph; the true radial intensity distribution $S(r)$ was, in turn, determined from the distribution $S(X)$ by application of the Abel transform. The theoretical relation between the emission intensity S and the temperature T is given by

$$S \sim n_H \exp(-E/kT) \qquad (2)$$

where n_H is the number of hydrogen atoms per unit volume, E the energy of the excited state, and k Boltzmann's constant. The intensity S reaches a maximum at a specific temperature T^* because the value of the atom concentration n_H decreases, and the exponential term increases as T increases. Thus, the temperature at the maximum point of the radial intensity distribution is T^*, and temperatures at other radial locations may be determined from a normalized curve of Eq. (2). Details of this procedure are presented in a recent paper by Kimura and Kanzawa.[5] The temperature on the axis of the central column passing through the constrictor of an arc engine operating at a current of 150 amps was estimated to be above 25,000°K.

Fastax motion pictures of the column through the quartz constrictor obtained at framing rates of 2000 and 7000 frames/sec revealed no interruption of the visible discharge.

C. Quantitative Analysis of the Central Core

For analysis in terms of the core flow model, the flow passing through the engine is subdivided into a core, inner, and outer flow. The core flow is defined as that portion of the total flow which is electrically conducting and in which energy is liberated due to joule or ohmic heating; the inner flow is defined as that portion of the total flow which receives energy from the core and is not electrically conducting; finally, the outer flow is defined as that portion of the total flow which receives energy directly from the constrictor wall but not from the column. As a working hypothesis, based on the observation that the diameter of the visible core appears constant, it is assumed that the longitudinal energy flux gradient along the central core is small. Following the original analysis of Suits,[1] the core flow is treated as if it were a hot cylindrical body. In Suits' analysis radiation was neglected, and semiquantitative relations were used to describe column behavior. In the present analysis radiation has been considered, and the behavior of the hot core has been based on exact numerical solutions for a fully developed laminar column.

The energy balance equation for a fully developed laminar column is based on the following assumptions: 1) column properties are functions only of radial distance from the axis and not of azimuthal position, and the longitudinal energy gradient along the column core is negligible; 2) local equilib-

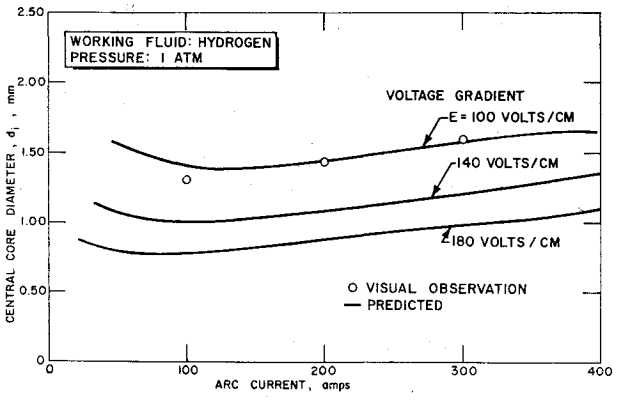

Fig. 8 Column diameter vs arc current and voltage gradient for a fully developed laminar hydrogen column at 1 atm pressure. The column diameter is based on the column 0°K isotherm.

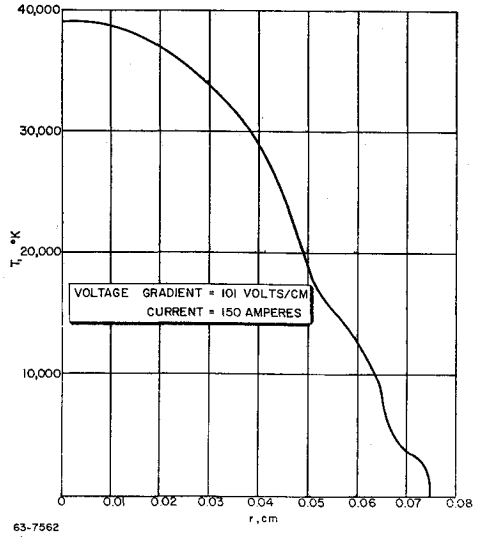

Fig. 9 Temperature vs radius for a fully developed laminar hydrogen column at 1 atm pressure.

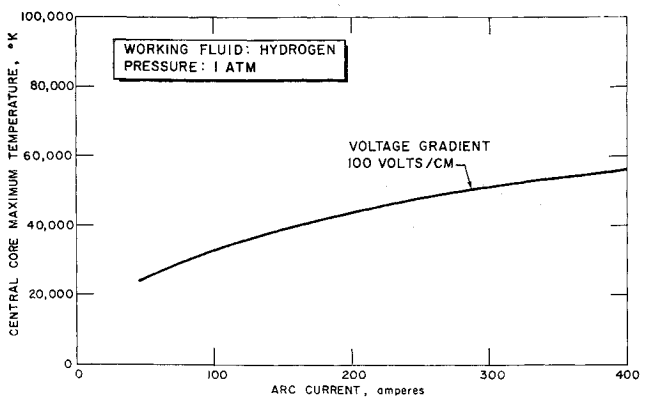

Fig. 10 Central temperature vs current for a fully developed laminar hydrogen column at 1 atm pressure and a voltage gradient of 100 v/cm.

rium holds everywhere in the column, and the column is optically thin; and 3) magnetohydrodynamic effects are small.

The energy balance for the laminar column (the Heller-Ellenbaas equation) has the form

$$\sigma E^2 = P_r - \frac{1}{r}\frac{d}{dr}\left(rK\frac{dT}{dr}\right) \tag{3}$$

where σ is the local electrical conductivity, E the local voltage gradient, P_r the local radiated power per unit volume, r the radial coordinate, K the local thermal conductivity, and T the local temperature. The quantities σ,K, and P_r are functions of temperature and pressure. These have been evaluated for hydrogen up to 100,000°K by Yos.[6] Equation (3) was solved numerically with the boundary conditions $T = T_{max}$ at $r = 0$, and $dT/dr = 0$ at $r = 0$. Typical results are presented in Figs. 8–10.

Figure 8 presents a curve of central core diameter, defined by the column 0°K isotherm, as a function of current and voltage gradient for hydrogen at 1 atm pressure. Superimposed on the analytical results are experimental values of the hydrogen core diameter estimated from photographs of the arc discharge obtained through the quartz constrictor at a hydrogen flow of 0.25 g/sec. The observed values of the central core diameter appear to correlate best with a voltage gradient of 100 v/cm.

Photographic estimates of the column diameter are open to some question because of the difficulty of accurately calibrating photographic plates. This problem is to some extent alleviated in the case of a stable high-current arc column because of the steepness of the column temperature profile. Figure 9 presents a plot of temperature vs radius for a fully developed hydrogen laminar column at a voltage gradient of 101 v/cm and arc current of 150 amps. The temperature at the outer column boundary increases from 0° to 7500°K in a radial distance of only a 0.1 mm.

Figure 10 shows maximum central column temperature vs arc current for a fully developed laminar hydrogen arc column at 1 atm pressure and a voltage gradient of 100 v/cm. The calculated central temperature of 40,000°K at an arc current of 150 amps is not incompatible with the central temperature of above 25,000°K estimated spectroscopically.

Questions basic to the understanding of the energy addition process are the following: 1) What fraction of the arc engine propellant flow passes through the arc discharge? 2) What is the axial energy flow rate through the arc discharge?

The central column longitudinal mass and energy flow rates at any station x along the discharge can be found from

$$\dot{m}_{col} = 2\pi \int_0^{r_0} \rho U r\, dr \tag{4}$$

$$P_{col} = 2\pi \int_0^{r_0} \rho U r h dr \tag{5}$$

where $\dot{m}_{col}$ is the column mass flow rate, P_{col} is the column energy flow rate, and r_0 is the column diameter. The assumption that the central core is a fully developed laminar column with local thermodynamic equilibrium allows evaluation of the density ρ and enthalpy h as functions of the temperature and, hence, of the radius r. However, in order to evaluate the integrals in Eqs. (4) and (5), it is also necessary to specify the local longitudinal velocity U. For illustrative purposes, the mass and energy flux integrals have been evaluated at the entrance to the exit nozzle. At this point it seems reasonable to assume that the local flow velocity is close to sonic. The results of a set of calculations showing column mass and energy flow rate as a function of current and voltage gradient for a 1-atm, sonic, fully developed laminar column are presented in Figs. 11 and 12.

Referring to Fig. 11, the column mass throughput is relatively small, being of the order of 0.01 g/sec compared to the typical hydrogen flow for a 30-kw arcjet engine of the order of 0.25 g/sec. The fraction of the total mass throughput which flows longitudinally through the discharge column of a 30-kw arcjet engine is, in general, a smaller fraction than 10% of the total mass flow. In contrast, even though the column mass flux is small, Fig. 12 shows that the column energy throughput can be appreciable and, in fact, a significant fraction of the total energy input. This result has important implications in terms of the energy release pattern along the arc discharge.

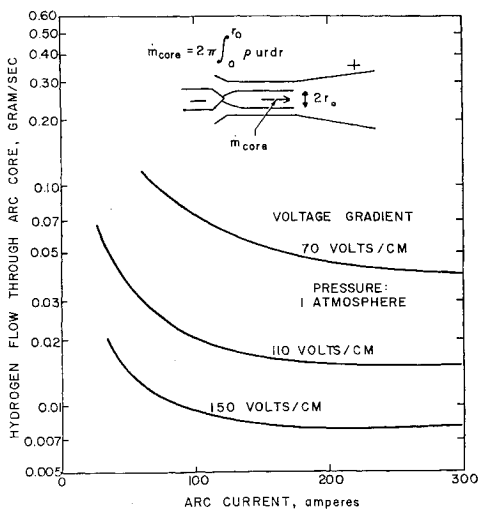

Fig. 11 Mass throughput vs current and voltage gradient for a 1 atm fully developed hydrogen laminar column.

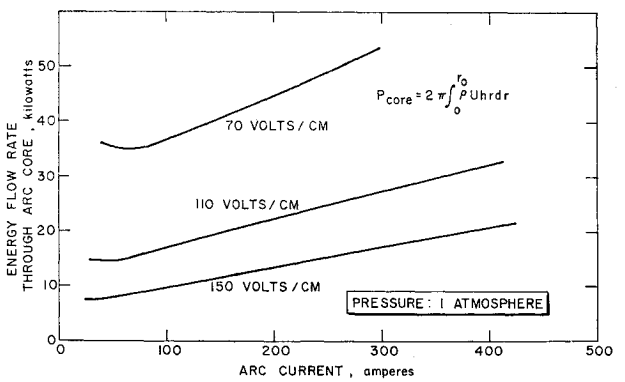

Fig. 12 Energy throughput vs current and voltage gradient for a 1 atm fully developed hydrogen laminar column.

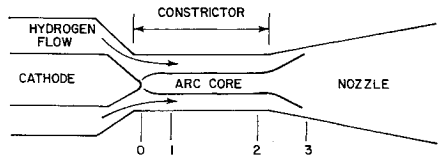

REGION 0-1 : ENERGY RELEASED DUE TO JOULE HEATING REMAINS WITHIN CORE. REGION OF HIGH VOLUMETRIC ENERGY RELEASE AND VOLTAGE GRADIENT.

REGION 1-2 : ENERGY RELEASED DUE TO JOULE HEATING IS CONDUCTED RADIALLY OUT OF CORE. AXIAL ENERGY FLUX GRADIENT IS SMALL.

REGION 2-3 : ARC ATTACHES IN LOW PRESSURE REGION OF NOZZLE.

Fig. 13 Model of the energy transfer pattern in an arc engine constrictor.

Referring to Fig. 13, the discharge region can, at least conceptually, be broken into three subregions. In region 0-1, which extends from the cathode tip into the constrictor, the voltage gradient and local volumetric rate of energy release are probably many orders of magnitude greater than the voltage gradients (100 v/cm) and volumetric energy release rates (1 Mw/cm^3) characteristic of a fully developed laminar column. All the energy released due to joule heating remains within the discharge, and there is a large longitudinal axial energy flux gradient. Region 1-2, which extends along the major portion of the constrictor length, is the luminous column visible in Fig. 7. All of the energy released due to joule heating in region 1-2 is probably conducted radially out of the column into the surrounding gas flow. As a result, even though the value of the longitudinal energy transport through the column is significant, the column axial energy flux gradient is small. Finally, region 2-3 is the low-pressure diffuse anode attachment region.

D. Engine Heat-Transfer Pattern

A basic premise of the core-flow model is that a portion of the working fluid is heated not by direct contact with the arc discharge but by contact with the hot engine walls. Information on the power that can be transferred by this heating mechanism may be obtained from an analysis of engine cool-off data.

Experimental values of engine thrust after power cut-off are plotted in Fig. 14. In this experiment, the hydrogen flow was held constant at its normal steady-state value, e.g., 0.10 g/sec, during the engine cool-down period. Three hundred seconds after power cut-off, the engine thrust is about 50 g, still an appreciable fraction of the steady-value of 150 g. During the cool-down period, the radiation-cooled engine is, of course, performing like a resistojet. The total energy content of the tungsten engine structure at power cut-off was estimated to be 750 kw-sec, which is in reasonable agreement with the value of 730 kw-sec calculated from the sum of the total energy radiated from the engine during

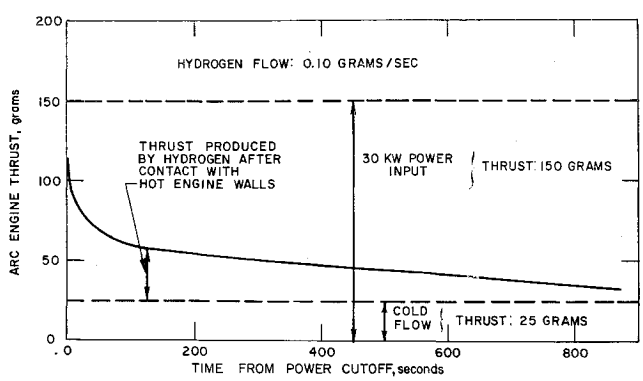

Fig. 14 Arc engine thrust vs time from power cut-off.

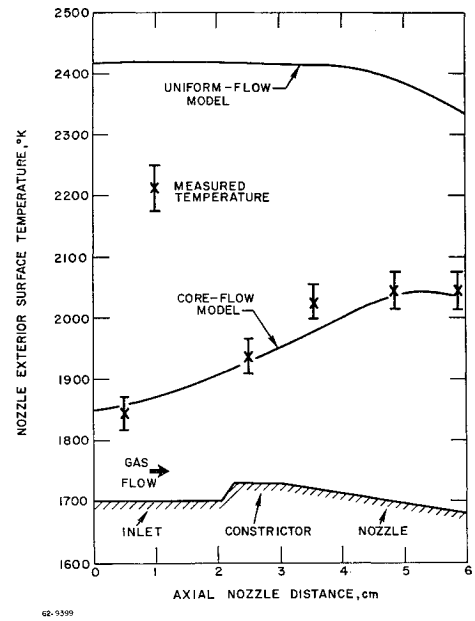

Fig. 15 Comparison of predicted and measured arc engine exterior surface temperature distribution.

cool-off (60 kw-sec) and the total energy transferred to the working fluid (670 kw-sec). The closeness of this agreement is probably fortuitous. Nevertheless, it does suggest that a significant portion (10 to 20%) of the input power can be transferred along a regenerative cooling path to the cold incoming propellant.

Further evidence of the existence of a conductive cooling path has been obtained from a steady-state heat conduction analysis of a 30-kw radiation-cooled arcjet engine. Figure 15 compares predicted and experimental engine exterior surface temperature distributions. In the case of the uniform or one-dimensional flow model, it is assumed that energy is simply transferred from the arc-heated gases to the engine wall. For the core flow model, it is assumed that there is a conduction heat flow path from the nozzle wall back into the constrictor. The calculated exterior surface temperature profile for the one-dimensional flow model reaches a maximum near the center of the engine; in contrast, the temperature profile for the core flow model reaches a maximum near the engine exit plane. The general shape of the measured engine exterior temperature distribution, as shown in Fig. 15, cannot be matched by the assumption of uniform flow, giving further credence to the suggestion that a heat-transfer path exists between the hot engine nozzle and the incoming cold gas.

E. Frozen and Nonuniform Momentum Flow Losses

In the interpretation of thermal arcjet engine performance, it is found convenient to define an arc, a frozen flow, and a nozzle expansion efficiency.

The arc efficiency is defined as the ratio of the total power delivered to the working fluid to the total power delivered to the engine, or

$$\epsilon_{arc} = \frac{P_{input} - P_{radiation}}{P_{input}} = \frac{P_{gas}}{P_{input}} \qquad (6)$$

where P_{input} is the electrical power input, and $P_{radiation}$ is the power radiated from the engine exterior surface. Physically, the arc efficiency is determined by convective heat transfer and electrode losses.

The frozen-flow power loss P_{frozen} is the power vested in the dissociated and ionized species flowing through the arc engine nozzle exit plane. The frozen-flow efficiency is defined as the ratio of power available for producing useful thrust at

the nozzle exit plane to the total power delivered to the working fluid, or

$$\epsilon_{frozen} = \frac{P_{input} - P_{radiation} - P_{frozen}}{P_{input} - P_{radiation}} = \frac{P_{available}}{P_{gas}} \quad (7)$$

The nozzle expansion power loss $P_{expansion}$ is the difference between the power available for producing useful thrust at the nozzle exit plane $P_{available}$ and the actual thrust power P_{thrust}. The nozzle expansion efficiency, a measure of the efficiency of conversion of available power to useful thrust power, becomes

$$\epsilon_{nozzle} = \frac{P_{input} - P_{radiation} - P_{frozen} - P_{expansion}}{P_{input} - P_{radiation} - P_{frozen}} = \frac{P_{thrust}}{P_{available}} \quad (8)$$

Finally, the over-all conversion efficiency is defined as the ratio of useful thrust power P_{thrust} to the input power P_{input}:

$$\epsilon_{over\text{-}all} = P_{thrust}/P_{input} \quad (9)$$

or

$$\epsilon_{over\text{-}all} = \epsilon_{arc}\, \epsilon_{frozen}\, \epsilon_{expansion} \quad (10)$$

Because of the complexity of the energy exchange processes, exact analytical and experimental determination of the individual energy conversion efficiencies is beyond present technology. However, notwithstanding the complexity of the situation, it is possible to understand qualitatively the nature of the energy loss mechanisms.

As the incoming propellant flow passes through and around the arc discharge, a fraction of the working fluid is dissociated into atoms, and a fraction of these atoms and of the undissociated molecules are, in turn, ionized into ions and electrons. At the entrance to the engine exit nozzle, an appreciable fraction of the electrical input energy is vested in the dissociation and ionization degrees of freedom of the working fluid. If the nozzle flow remains in equilibrium, i.e., the dissociated and ionized species recombine during the nozzle expansion process, all of the power delivered to the working fluid is available for producing directed kinetic energy or thrust. On the other hand, if the nozzle flow is frozen, i.e., the dissociated and ionized species do not recombine during the nozzle expansion process, then all of the energy vested in the dissociation and ionization degrees of freedom will be lost. One-dimensional numerical analyses of the nozzle expansion process, using the most recent data on hydrogen atom and ion-electron recombination, indicate that there is little hope for significant recombination of dissociated molecules or ionized atoms during the nozzle expansion process.[7] Furthermore, even if a catalyst could be found to accelerate the recombination process significantly (which appears unlikely), the required nozzle lengths would be excessive, and wall friction losses would tend to overwhelm the energy addition due to recombination.[7, 8] In the same vein, spectroscopic measurement close to the exhaust plane of the 30-kw engine have indicated average electron concentrations of 10^{15} electrons/cm^3 and local electron concentrations at the center of the exhaust jet as high as 10^{16} electrons/cm^3. These values of the electron concentration are many orders of magnitude greater than the values that would be characteristic of equilibrium flow in the arcjet engine exhaust nozzle.[8] Thus, both analytical and experimental results indicate that the nozzle flow is probably completely frozen.

In the core-flow model of the arc engine energy addition process, only a portion of the total propellant flow is heated by direct contact with the arc discharge; the remainder of the propellant flows coaxially with the arc discharge and is heated by direct contact with the hot tungsten walls. Figure 16 presents a calculated curve of hydrogen frozen flow efficiency at 1 atm pressure as a function of hydrogen temperature. The frozen flow efficiency is based on the assumption

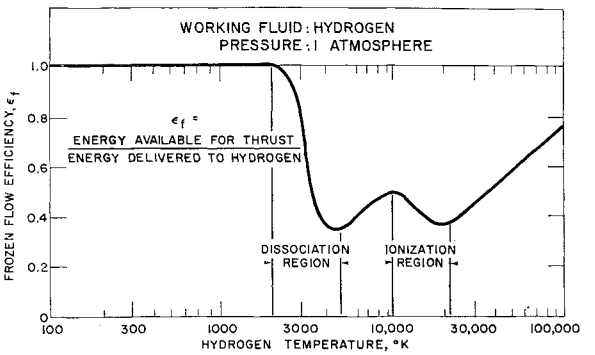

Fig. 16 Hydrogen frozen flow efficiency vs hydrogen temperature at 1 atm pressure.

that the energy vested in dissociation and ionization is not recoverable. As the hydrogen temperature is increased, the frozen flow efficiency initially decreases corresponding to the dissociation of hydrogen molecules. At about 5000°K the hydrogen molecular dissociation is complete, and further increase in temperature increases the frozen flow efficiency. From 10,000° to 22,500°K there is another fall in frozen flow efficiency corresponding to energy absorption in hydrogen atom ionization. For the core flow model, the cold gas that is in direct contact with the engine wall can have a frozen flow efficiency close to unity; the gas in immediate contact with the discharge can, in turn, have frozen flow efficiencies as high as 50% and even greater. It is thus postulated that in some circumstances the existence of nonuniform flow at the entrance of the arc engine nozzle might increase the fraction of thermal energy over that characteristic of the uniform flow situation.

Referring to Fig. 16, the frozen flow efficiency can range in value from 35% to nearly 100%. Since the nozzle flow is probably frozen, the major difficulty in predicting the frozen flow efficiency is that of establishing the energy actually absorbed in the dissociation and ionization degrees of freedom during the gas electrical heating process.

The core flow model of thermal arcjet engine energy addition predicts that nozzle inlet conditions will be highly nonuniform. Strong radial gradients are predicted in temperature, density, and velocity. Figure 17 indicates hydrogen frozen flow specific impulse as a function of hydrogen temperature. In terms of the core-flow model, the hydrogen that is not in contact with the column is heated by the engine walls to gas temperatures corresponding to the specific impulse range from 500 to 1000 sec; on the other hand, the gas that is in direct contact with the arc discharge is heated to hydrogen temperatures corresponding to specific impulses from 1000 to 5000 sec and, perhaps, even greater. The flow at the nozzle entrance is thus composed of a series of coaxial stream tubes, each characterized by a different local mass flux and thermal energy content. If the different streams fail to mix during the nozzle expansion process, there can be an appreciable thrust loss compared to the uniform flow situation.

To illustrate the potential thrust loss, Fig. 18 presents predicted values of engine thrust for a highly simplified two-fluid model of the nozzle inlet flow pattern. Engine thrust is plotted as a function of the ratio of fluid 1 flow rate to the total flow rate. The total hydrogen flow rate is 0.10 g/sec. Of the total input power of 30 kw, 25 kw are assumed to be transferred to fluid 1 and 5 kw to fluid 2. The two streams are assumed not to mix with each other; however, the energy in each of the streams is assumed to be converted into kinetic energy. The total thrust level increases steadily, reaches a peak, and then decreases as the mass flow of fluid 1 is increased. The maximum thrust is obtained when the ratio of mass flows between the two streams is equal to the ratio of power supplied to the two streams, i.e., uniform flow. For

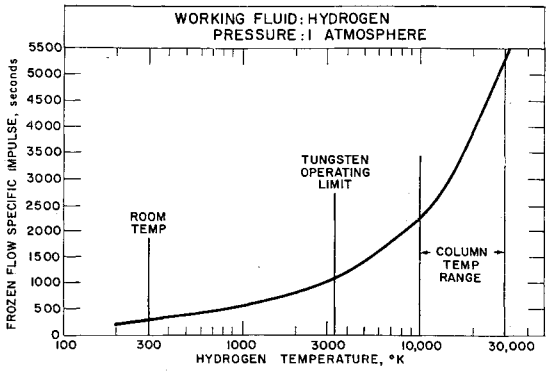

Fig. 17 Hydrogen frozen flow specific impulse vs hydrogen temperature at 1 atm pressure.

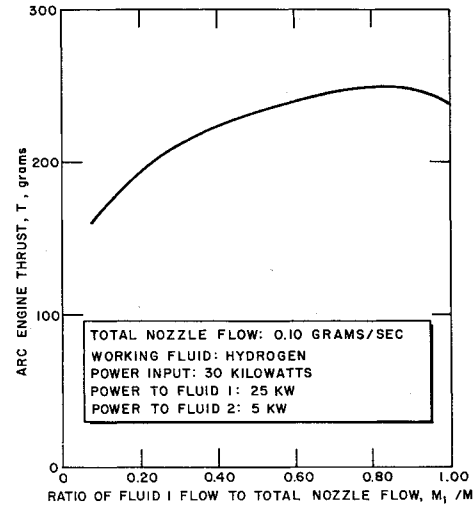

Fig. 18 Engine thrust vs the ratio of flow 1 to total flow. Of the total power input of 30 kw, 25 kw are transferred to the inner flow and 5 kw to the outer flow. The flow is assumed to be in equilibrium, and the two streams do not mix.

frozen flow the thrust maximum occurs at a different mass flow apportionment.

Other sources of momentum loss during the nozzle expansion process are associated with boundary-layer buildup along the nozzle walls[8] and with the fact that an arc engine must have a finite exit nozzle area ratio.[7] In the latter case, thermal energy is passed out of the exit nozzle before it can be converted to useful thrust power.

F. Experimental Determination of Arc Engine Power Losses

Estimated values for the different energy conversion efficiencies are summarized in Table 3. Referring to Table 3, until quite recently the main emphasis in the measurement of arc engine propulsion performance has been the measurement of over-all energy conversion efficiency and the arc efficiency by calorimetric measurement of the exhaust power or measurement of energy radiated from the engine surface. The power vested in ionization, dissociation, and momentum losses has, however, usually been considered together in one term. If a physical understanding of the effects of changes of arc engine geometry on propulsion efficiency is to be obtained, it is necessary to be able to separate the power absorbed in ionization and dissociation from the power absorbed in momentum losses.

Probably the most direct method for accomplishing this separation is to obtain a systematic aerodynamic characterization of the arc engine exit jet flow as a function of operating conditions and engine geometry. Aerodynamic characterization of the exit jet is defined as the determination of local flow velocity, local stagnation and static pressures, and local mass flux. Knowledge of these quantities will permit a direct measurement of the power vested in directed kinetic and translational energy of the gas. When compared with the measured thrust and cooling powers, this will lead to the possibility of separating the nozzle expansion and frozen flow losses.

IV. Summary and Conclusions

1) A useful lifetime of one month has been established for a hydrogen radiation-cooled arcjet engine operated at a specific impulse of 1000 sec, input power of 30 kw, and over-all electric-to-thrust power conversion efficiency greater than 40%. Reliable radiation-cooled engine operation at the 30-kw power level and at electric-to-thrust power conversion efficiencies of 40% has been obtained with hydrogen at specific impulses up to 1500 sec and with ammonia up to 1000 sec. Specific impulses greater than 2000 sec at 35% efficiency have been obtained with a radiation-cooled hydrogen arcjet engine operated at a power level of 200 kw.

2) A core-flow model has been proposed to describe the mechanisms of energy addition in a radiation-cooled thermal arcjet engine with a constricted arc configuration. A portion of the gas flow passing through the engine is heated by direct contact with the engine walls, and the remainder is heated by direct contact with the arc discharge. Photographic observations obtained through a quartz constrictor, in confirmation of the core flow model, indicate that there is a smooth, constant-diameter, luminous core, extending from the cathode completely through the constrictor to the anode. Analysis of experimental engine cool-off data and exterior surface temperature distributions demonstrates, again in agreement with the core flow model, the existence of a conductive heat-transfer path from the hot engine walls to the cold incoming propellant.

3) The experimental verification of the existence of a core flow within the arc engine constrictor indicates that energy can be transferred to the arc engine working fluid with a minimum degree of contact between the arc-heated gases and the engine walls. This mechanism of energy transfer alleviates the arc engine material problem and offers a rational basis for believing that the arc engine still has considerable specific impulse growth potential.

4) Until quite recently, the main emphasis in the measurement of arc engine propulsion performance has been the direct measurement of electrical power input power lost from the engine exterior surface and thrust power. The power vested in ionization, dissociation, and momentum losses has been considered together in one term. In order to obtain a physical understanding of the energy exchange processes, the next step is to separate clearly the power absorbed in frozen flow losses from the power absorbed in momentum losses.

5) Analysis of the discharge passing through the constrictor suggests that there is a region of high volumetric energy release in the vicinity of the cathode tip. The determination of the portion of the total input power released in the cathode tip region and the portion released in the column can best be established by direct measurements of the column voltage gradient.

Table 3 Arc engine energy conversion efficiencies

Arc efficiency	0.80 to 1.00
Frozen flow efficiency	0.35 to 1.00
Nozzle expansion efficiency	0.60 to 0.95
Over-all efficiency	0.20 to 0.50

References

[1] Cobine, J., *Gaseous Conductors* (Dover Publications, New York, 1958), pp. 162–168 and 339–343.

[2] Jack, J. R., "Theoretical performance of propellants suitable for the electrothermal jet engine," ARS J. **31**, 1685–1689 (1961).

[3] Larentz, W., "Uber ein verfahren zur messung sehr hoher temperaturen in nahezu durchlässigen bogensaulen," Z. Physik **129**, 327–342 (1951).

[4] Olsen, H. N., "Thermal and electrical properties of an argon plasma," Phys. Fluids **2**, 614–623 (1959).

[5] Kimura, I. and Kanzawa, A., "Measurement of stream velocity in an arc," AIAA J. **1**, 310–312 (1963).

[6] Yos, J., "Theoretical and experimental investigation of arc plasma—Generation technology, Part II, Applied Research on electric arc phenomena," Aeronaut. Systems Div., Wright Field, Dayton, Ohio, ASD TRD 62-729, pp. 87–167 (1963).

[7] Mironer, A. and Macomber, H., "Chemical nonequilibrium effects in thermal arc jet propulsion," *AIAA Progress in Astronautics: Electric Propulsion Development*, edited by E. Stuhlinger (Academic Press, New York, 1963), Vol. 9, pp. 121–147.

[8] Chen, M., "Effect of nonequilibrium flow in thermal arc jet engines," RAD-TR-62-25, NASA Lewis Research Center (September 1962).

NOVEMBER 1963 AIAA JOURNAL VOL. 1, NO. 11

Computer Simulation of the Electron Mixing Mechanism in Ion Propulsion

O. Buneman*
Stanford University, Stanford, Calif.

AND

G. Kooyers†
Litton Industries, San Carlos, Calif.

A one-dimensional simulation with electrons and ions treated as sheet charges in mutual coulomb interaction and simplified emission conditions (ions are injected with uniform velocity through a plane accelerator grid, electrons with a thermal distribution from a plane decelerator grid at ship potential) was programmed into a digital computer. The dynamic buildup of the plasma is observed; the thrust seems to be maintained almost steadily, and good spontaneous neutralization seems to take place. Nonstatic space charge fields oscillating at the electron plasma frequency seem to provide the entropy increase needed for proper mixing.

I. Introduction

THE subject of neutralization has been approached with a wide range of attitudes that have resulted in varying degrees of optimism and pessimism.

Instinctively, one feels that the heavy ions will always pull along the requisite number of electrons, provided they are made available from some source placed in or near the beam. Any unbalance of charge will result in electrostatic fields that redistribute electrons in such a way as to restore neutrality. Indeed, it would appear that this mechanism is not dependent on collisions for its operation, and the scarcity of collisions cannot be invoked against one's "instinctive" confidence in successful neutralization.

However, careful and rigorous analytical studies have been made of the problem of collision-free electron-ion mixing. They have, on the whole, yielded negative results.[1] Broadly speaking, it is found that the electrostatic field mechanism for the adjustment of electron densities results in "overshooting" by the electrons and, at best, only neutrality in-the-mean has been achieved in rigorous theoretical models of the mixing problem.[2] Whenever the electrons are released with velocities more than twice the ion velocities (and in ion engines one would want to release them with possibly three times the ion velocity), theory has failed altogether to provide a rigorous solution, i.e., a selfconsistent field distribution in the beam.

This is one cause of possible pessimism regarding efficient mixing, and extensive experimental research was devoted to checking the theoretical predictions. On the whole, these experiments have resulted in reversion to optimism and even complete disregard of the problem. The experiments, on the other hand, encountered the criticism that space conditions cannot be simulated properly in the laboratory, and distant boundaries seemed to play a major role in the theories.

In the meantime, further theoretical developments have not been able to settle with certainty the argument whether and how neutralization may occur. The search has continued for a static potential distribution in the neutralizer region, taking into account more complicated effects. The original calculations had been concerned with monoenergetic electrons and ions and had, at best, resulted in spatially varying po-

Presented at the AIAA Electric Propulsion Conference, Colorado Springs, Colo., March 11–13, 1963; revision received August 30, 1963. This work was done under NASA Contract No. NAS-3-2503. The authors would like to acknowledge the assistance of David Brauch and Patricia Vartanian in writing the computer program and of Gerold Pokorny for helpful discussion of the one-dimensional formulation.

* Professor of Electrical Engineering; also Consultant, Litton Industries, Electron Tube Division.

† Senior Engineer, Research Department, Electron Tube Division.